POAC'15
Trondheim, Norway

Proceedings of the 23rd International Conference on
Port and Ocean Engineering under Arctic Conditions
June 14-18, 2015
Trondheim, Norway

TENTATIVE FRACTURE MECHANISMS OF THE PARALLEL CHANNEL EFFECT DURING ICE MANAGEMENT

Wenjun Lu, Raed Lubbad, Sveinung Løset
SAMCoT, NTNU, Trondheim, Norway

ABSTRACT

During an ice management operation, parallel channels were often created by the operating icebreakers. Because of the close-by free boundary effect induced by a neighbouring parallel channel, large cracks may form linking these parallel channels. These large cracks intersect the solid ice in between and generate smaller broken ice floes. This is beneficiary for an effective ice management operation. This phenomenon has been frequently observed and recognised in various field tests and reported in scientific publications. However, up to now, there exist no theoretical explanations behind this 'parallel channel effect'. As an initial step towards addressing practical problems in relation to 'the optimum parallel channel spacing' and 'the out-going floe size' for certain ice management patterns, we present in this paper a theoretical model based on fracture mechanics to account for the repetitively observed two types of cracks, i.e., the side and front cracks. Based on both field observations and theoretical analysis, we found that this theoretical model offers reasonable predictions. In addition, different behaviour and characteristics of side and front cracks were identified, e.g., front cracks tend to kink toward the nearest free boundaries at an angle of about 50^o, side cracks show a strong tendency of kinking away from the free boundary with an angle of 90^o. Furthermore, for the sake of enhancing the parallel channel effect, geometrical considerations such as the requirement on the parallel channel's spacing and the aspect ratio of out-going broken ice floes were addressed in a ratio format in this paper. Further quantifications of these practical problems can be built upon such information in separate studies.

1. INTRODUCTION

One of the important objectives of a physical ice management operation is to reduce the invading ice floes' size. This can be achieved via different ice management strategies. Typically, several icebreakers are hierarchically deployed and operate with different patterns to systematically break the incoming large ice floes. These include circular, elliptical, racetrack, orbital and linear patterns (Hamilton et al., 2011a). Among all these different patterns, the importance of 'parallel channel effect' in reducing the floe size has been observed and recognised (Farid et al., 2014; Hamilton et al., 2011a). During an ice management operation, an icebreaker opens a channel behind it. In a reference system moving with the drifting ice floe, due to icebreakers' 'back-and-forth' patterns, the successive channel can be influenced by the previous channels. It has been frequently observed that large cracks were formed linking two neighbouring channels together (see Figure 1). These large cracks intersect the solid ice in between parallel channels and produce certain sized ice floes.

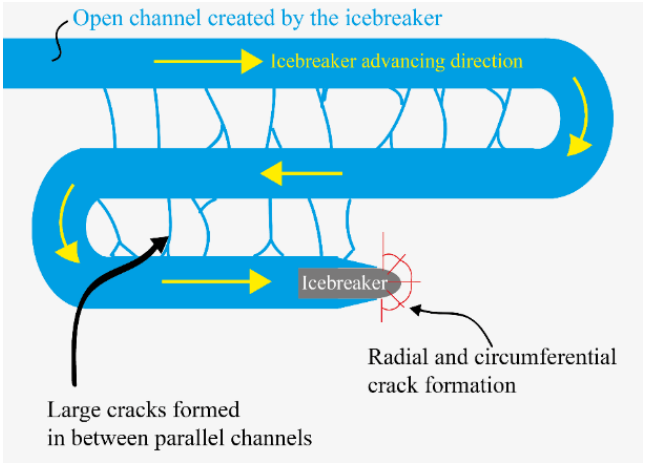

Figure 1. Illustration of the parallel channel effect during an ice management operation.

Such ice fracturing phenomena is rather important while designing the fleet deployment during an ice management operation. Hamilton et al. (2011a; 2011f) developed a numerical simulator based on kinematics to quantify the performance of different ice management strategies. One critical assumption behind the simulator is that ice floes of an aspect ratio of 1:1 are generated between two parallel channels. This assumption based mainly on field observations, as there exist no theoretical explanations. This paper seeks to offer some tentative explanations of the fracture mechanisms behind the parallel channel effect. The theoretical formulation can serve as an initial step towards addressing practical questions such as 'optimised parallel channel spacing' and 'out-going floe size' for specific ice management operations. Moreover, implementing such fracture mechanical models into the current multibody dynamic simulator (Lu, 2014; Lubbad and Løset, 2011) can further enhance the evaluation of different ice management strategies.

This paper starts with field observations regarding the parallel channel effect. Based on observations documented in Section 2, we selected two types of cracking events, which we consider as two of the most significant contributions to the parallel channel effect, for further theoretical analysis. Theoretical models were introduced in Section 3 followed by results and discussions in Section 4 and 5 respectively. Eventually, we offered a theoretical model whose predictions are in line with field observations and some conclusions were drawn during the developing process.

2. OBSERVATIONS

For an icebreaker transiting in a broken ice field composed of large ice floes, we often observe large cracks formed and propagating for a significant distance. Classic theories regarding radial and circumferential cracks' formation within a semi-infinite ice floe (Kerr, 1976; Nevel, 1958; Nevel, 1961; Nevel, 1965) are insufficient to explain phenomena as such (see the 'red' cracks in Figure 1). Free boundaries pose great influences to the fracture pattern of sea ice (Lu, 2014). Since 2012, extensive monitoring systems on board of different icebreakers have been utilised by the research group of SAMCoT[1] to observe the formation and propagation of these 'large' cracks (Lubbad, 2012; Lubbad et al., 2012; Lubbad et al., 2013a; Lubbad et al., 2013b). Particularly in 2013, a 360º camera system was installed on board of ODEN and rather satisfactory interaction processes and ice conditions were continuously documented with panoramic images (Bjørklund et al., 2015; Scibilia et al., 2014). In addition, parallel channel effect has been tested in the same 2013 research cruise (Farid et al., 2014).

Rather chaotic processes were perceived by a first glance of all the large cracks' formation and propagation documented by the 360º camera system. However, if we pay attention, some general trends can be isolated from these chaotic pictures. In the following sections, we present two groups of cracks' formation and propagation. We believe that they are among the most important fracture mechanisms behind the parallel channel effect.

2.1 Side cracks

Figure 2.1 illustrates that ODEN is entering a 300 m wide ice floe. After some distance of penetration, Figure 2.2 shows the development of a crack in ODEN's starboard side. Notably, this starboard side crack kinks into the large ice floe. In Figure 2.3, a similar port side crack was developed and kinks into the large ice floe. Figure 2.4 shows the final opening of these two side cracks. In addition, a new slanted crack formed and merged into the existing starboard side crack.

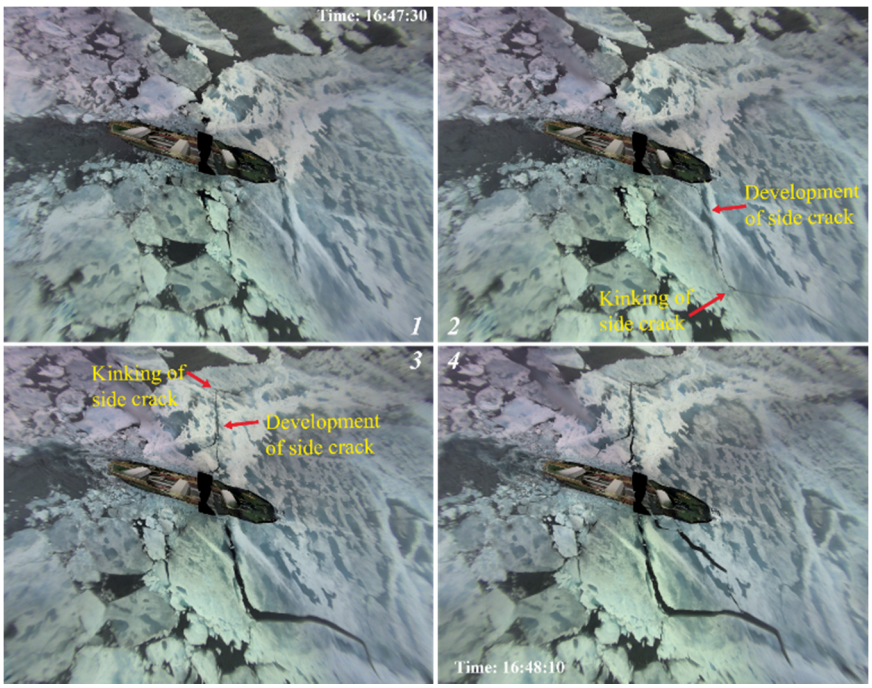

Figure 2. Side cracks' formation and propagation within an ice floe of approximately 300 m in width (360º camera system images on Aug 28th, 2013).

[1] SAMCoT stands for Sustainable Arctic Marine and Coastal Technology and is a research centre based in Norwegian University of Science and Technology.

2.2 Front cracks

Immediately following the interaction processes in Figure 2 (see the time mark in Figure 3.1), a front crack was developed at the bow area of ODEN as in Figure 3.2. Interestingly, this front crack 'choose' to kink into its right-hand-side direction, which presents a shorter route to the free boundary (see Figure 3.3). This seemingly random behaviour was repetitively observed in the tests. Several other observations were also illustrated in Figure 4.

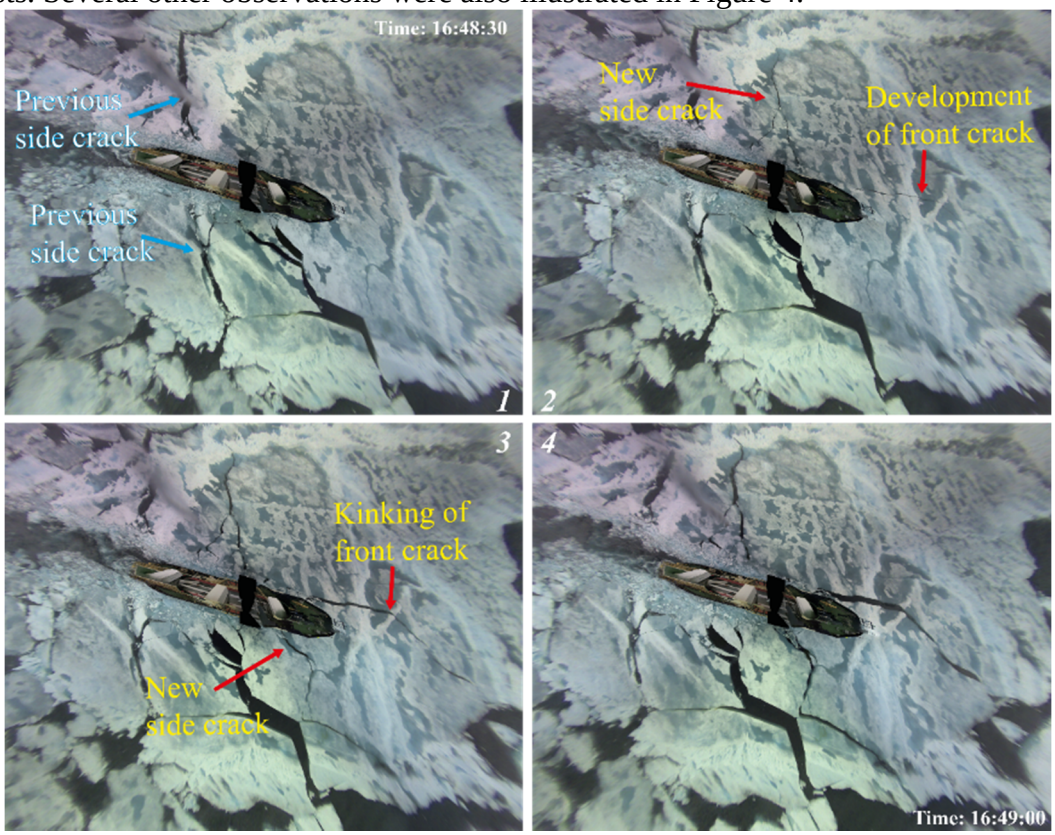

Figure 3. Front crack's formation and propagation within an ice floe of approximately 300 m in width (360o camera system images on Aug 28th, 2013).

In addition, similar as in Figure 2, Figure 3.2 and 3.3 also illustrated the formation and propagation of side cracks. These side cracks also displayed a tendency of kinking into the large ice floe.

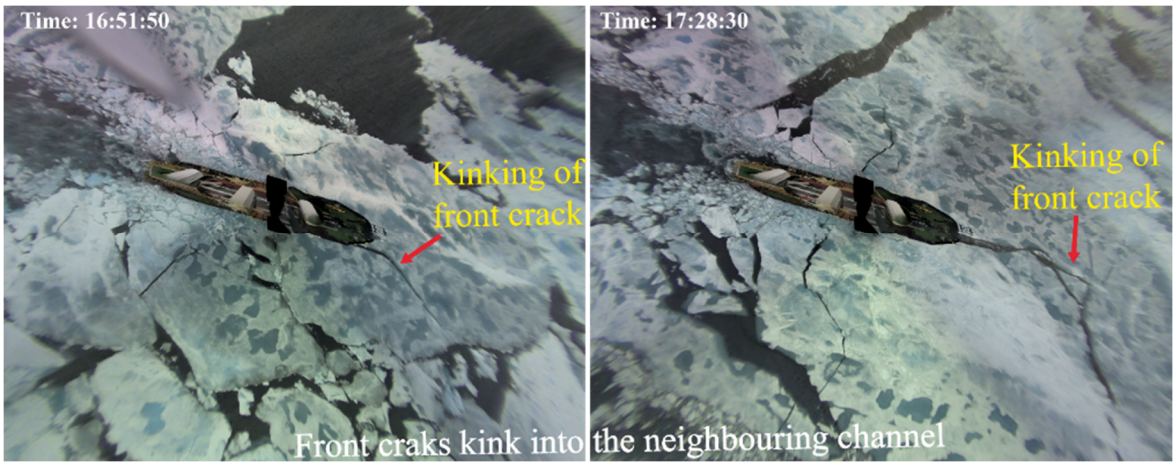

Figure 4. Repetitive observations of front crack kinking into the closest channel on August 28th, 2013.

All these important observations offer us precious opportunities to explore the physical mechanisms behind.

2.3 Summary of the observations

We believe that the mechanisms of these large cracks are all due to the presence of a mild/negligible confinement. Otherwise, the local failure would dominate (Lu et al., 2015h).

Based on the observations made in the test (as illustrated by Figures 3, 4 and 5), several important points can be drawn as in the following:

- Most cracks were initiated around the bow area. Very few cracks were initiated from mid-ship or astern;
- Ice fractures in a variety of patterns, which are influenced by factors such as inhomogeneity, irregular boundary, random radial crack formations, etc.;
- Among varying fracture patterns experienced by ODEN, we present two types of repetitively observed of cracks, i.e., the side and front cracks. They are both considered as sub-types of the previously studied in-plane fracture mechanism (Lu et al., 2015a);
- If the considered ice floe (or the channel spacing) is wide enough, side cracks show a tendency to kink into the large ice floe; otherwise, the side crack can just propagate through the ice floe;
- The presented front crack shows a strong tendency to kink into the free boundary direction;
- Based on the observations in Figures 3 and 4, we believe that both the side cracks and the kinking behaviour of front cracks are among the most important failure mechanisms behind the parallel channel effect.

In the next section, we present the physical mechanisms behind the side and front cracks following the concept of fracture mechanics. The analysis is built upon previous studies in terms of the out-of-plane and in-plane failure of an ice floe while interacting with a sloping structure (Lu, 2014).

3. FRACTURE MECHANICS MODEL

Theoretical models based on fracture mechanics are presented in this section to account for the observations in Section 2.

3.1 Overview of the fracture mechanisms

Ice fractures in a variety of ways while interacting with a sloping structure. Generally, we can categorise them into the ‘in-plane fracture (Lu et al., 2015a)’, ‘out-of-plane fracture (Lu et al., 2015e)’, or both (Lu et al., 2015h).

Out-of-plane radial cracking

Out-of-plane fracture mechanisms, however, cannot generate too long cracks (termed as radial cracks). The length of these radial cracks is limited by the formation of circumferential cracks. According to Finite Element Method (FEM) analysis, it was found that these radial cracks could not propagate further than 2 times the characteristic length ℓ of a floating ice plate (Lu et al., 2015e; Sodhi, 1996). This characteristic length can be approximated by Eq. (1) for typical ice material properties (Gold, 1971).

$$\ell = 13.5t^{3/4} \tag{1}$$

in which,

t is ice thickness [m];
ℓ is the characteristic length for a plate resting on an elastic foundation [m].

Therefore, for parallel channel spacing which is smaller than 2ℓ, radial cracks can feel the free boundary and propagate through. However, as the parallel channel spacing increases, a different failure mechanism, in-plane fracture, is believed to generate long enough cracks linking parallel channels.

In-plane fracture

Different from the out-of-plane fracture mechanism, in-plane fracture can propagate a crack several kilo-metres away as long as rather mild/negligible confinement are present (Lu et al., 2015a). Splitting failure has been studied as a pure Mode-I fracture by Lu et al. (2015). In this paper, in order to account for the side and front cracks' kinking behaviour (see Figures 3, 4 and 5), we extended the Mode-I in-plane fracture into Mixed Mode fracture scenarios.

3.2 Parallel channel effect due to in-plane fracture mechanism

Figures 2, 3 and 4 demonstrate that both the side and front cracks are much longer than the extent to which a radial crack can propagate. Therefore, it is fair to conclude that large cracks in Figures 2, 3 and 4 are primarily due to the in-plane fracture mechanism. Section 2.3 summarised important observations during the parallel channel test. Both the side and front cracks are largely influenced by the close-by free boundaries. Especially, the front crack shows a strong tendency to kink into the nearby free channel, thereby leading to the 'parallel channel effect'. We shall focus mainly on the in-plane fracture mechanism of these observed crack patterns, the theoretical models of which are presented in the following.

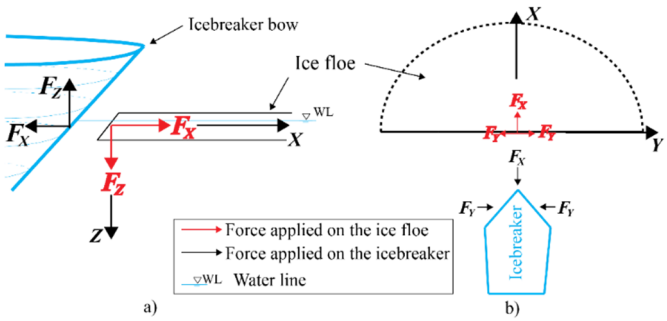

Figure 5. Coordinate system for the simplified contact model.

Coordinate system and contact model

Before any fracture takes place, during the initial contact between an icebreaker and an ice floe, we define the following coordinate system and corresponding contact force (see Figure 5). Similar as in a series of studies made in previous publications (Lu, 2014), we simplify the contact model by considering only the global contact force F_X and F_Y. A detailed analysis of the local contact mechanisms is beyond the scope of current study. Simplified geometric consideration and ice crushing limit are assumed sufficient in obtaining the global contact force's decomposition information. Therefore, these contact force can be conveniently related as in Eq. (2) by deterministic parameters β_{YX}, β_{XZ} and β_{YZ}. After the fracture has taken place, for the sake of studying crack propagation, we sometime need to isolate a small part of the contact region (more description regarding this will be offered in Section 3.2 in relation to Figure 7). This leads to partial contact forces $F_X^{'}$, $F_Y^{'}$, and $F_Z^{'}$. As a further simplification, we assume that these partial contact force components follow the same ratio parameters as in Eq.

(2). Though the contact force components have been largely simplified in this paper, the actual partial/full contact scenarios can be implemented numerically depending on the given structure and ice information.

$$\begin{aligned}\beta_{YX} &= \frac{F_Y}{F_X} = \frac{F_Y^{'}}{F_X^{'}} \\ \beta_{XZ} &= \frac{F_X}{F_Z} = \frac{F_X^{'}}{F_Z^{'}} \\ \beta_{YZ} &= \beta_{YX}\beta_{XZ} = \frac{F_Y}{F_Z} = \frac{F_Y^{'}}{F_Z^{'}}\end{aligned} \tag{2}$$

Theoretical model: side and front cracks' propagations

We utilised two theoretical models to study the side and front cracks' propagation in this paper. Figure 6 shows the theoretical model for a front crack's propagation. We assume that the front crack initiates at the stern of the ship bow. This is mainly because the stern has a higher chance to initiate such front crack based on the principle that the first radial crack initiation is normal to the edge of an ice floe (Kerr, 1976). Because the assumed front crack (before its kinking) locates in the symmetric line of the icebreaker's length direction, no special contact regions need to be isolated to study the crack propagation. Therefore, we have the same global contact force F_X and F_Y to drive the front crack's propagation in the theoretical model of Figure 6. However, this assumed front crack resides unsymmetrically within the considered ice floe. This leads to mixed mode Stress Intensity Factors (SIFs) at the crack tip of the front crack and its subsequent kinking behaviour.

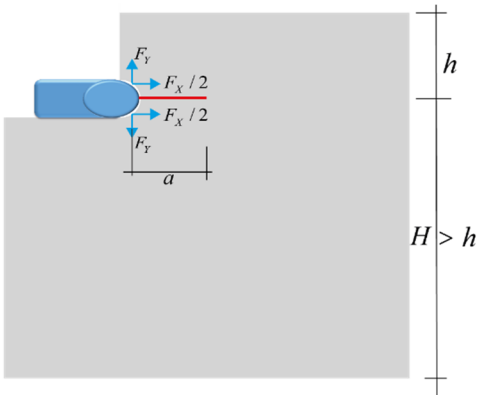

Figure 6. Theoretical model to study front crack's propagation.

Similarly, we adopt the theoretical model in Figure 7 to study side cracks' propagation. However, we lack information of its location of initiation. According to the observations made in Section 2.2, most cracks emanate from the bow region, i.e., only the bow region has contact with the intact ice floe; and side cracks can initiate at any location within its bow region. Suppose that the ship bow length is L_B, under the same coordinate system in Figure 5, the coordinate X_{side_crack} from which a side crack initiates must satisfy the condition in Eq. (3).

$$0 \le -X_{side\_crack} \le \min(L_B, h - X_{side\_crack}) \tag{3}$$

in which,

X_{side_crack} is the coordinate along the X axis at which side crack initiates (see Figure 7) [m];

L_B is the length of the bow region which has frequent contact with intact sea ice [m].

In light of the right hand side of Eq. (3), we further studied two scenarios of side cracks' propagation as depicted in Figure 7.

- Side crack scenario #1: $h > L_B + X_{side\_crack}$ (refer to Figure 7a);
- Side crack scenario #2: $h \le L_B + X_{side\_crack}$ (refer to Figure 7b).

In both scenarios, in order to study the side crack's propagation, a partial contact region has to be isolated to acquire the driving force for crack propagation. This leads to partial contact forces $F_X^{'}$ and $F_Y^{'}$ which we assume to be related by Eq. (2).

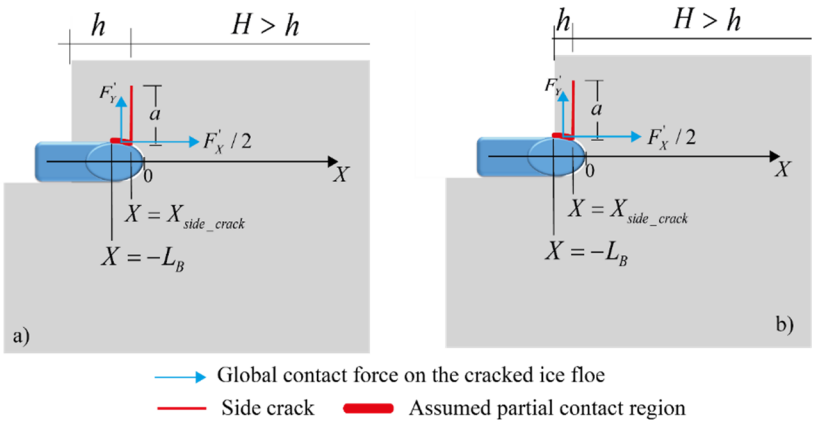

Figure 7. Theoretical model to study side crack's propagation.

3.3 The fracture mechanics model

The assumed theoretical models in Figures 6 and 7 can be generalised by the fracture mechanics model in Figure 8, in which an initial crack a locates unsymmetrically in a quarterly infinite plate. This crack is opened due to a turning moment M and a compressive force P. Because of its unsymmetrical location and loading conditions, mixed mode SIFs exist at the crack tip. This leads to the kinking of the initially straight crack. The kink angle θ is utilised to quantify this.

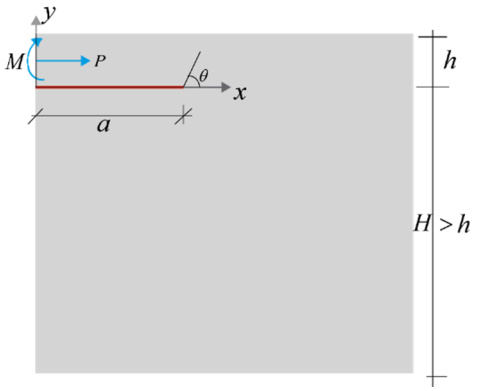

Figure 8. The fracture mechanics model utilised to study the side and front cracks' propagation.

The SIFs of such cracked geometry are available in literatures (Hutchinson and Suo, 1991; Thouless et al., 1987) as in Eq. (4).

$$K_I = \frac{\cos(52.07^o)}{\sqrt{2}}\frac{P}{t\sqrt{h}} + \sqrt{6}\sin(52.07^o)\frac{M}{t\sqrt{h^3}}$$
$$K_{II} = \frac{\sin(52.07^o)}{\sqrt{2}}\frac{P}{t\sqrt{h}} - \sqrt{6}\cos(52.07^o)\frac{M}{t\sqrt{h^3}} \quad (4)$$

in which, the physical meanings of each symbols are illustrated in Figure 8. The number 52.07° is deduced according to an idealised assumption $H >> h \to h/H = 0$. Though the fracture mechanic model of Figure 8 is assumed to be applicable to both side and front cracks' propagation problems, the exact formulation of P and M differs substantially for theoretical models in Figures 6 and 7. For the front crack propagation scenario, Eq. (5) relates the contact force with the fracture mechanics model.

$$P = F_X / 2$$
$$M = F_Y a - F_X h / 4 \quad (5)$$

For the side crack propagation scenario, Eqs. (6) and (7) relate the contact force with the fracture mechanics models in Figure 7a and b respectively, i.e.,

For side crack scenario #1, $h > L_B + X_{side\_crack}$:

$$P = F_Y^{'}$$
$$M = -F_Y^{'}[h/2 - (X_{side\_crack} + L_B)/2] - F_X^{'} a/2 \quad (6)$$

For side crack scenario #2, $h \le L_B + X_{side\_crack}$:

$$P = F_Y^{'}$$
$$M = -F_X^{'} a/2 \quad (7)$$

It is interesting to notice that the overturning moment M in both Eqs. (6) and (7) are negative. This is considered as the major reason that side cracks tend to kink into a different direction as oppose to the front crack (more on below).

3.4 Kinking of cracks under mixed mode loading

Kink direction

According to Thouless et al. (1987), depending on the sign of K_{II}, a crack kinks into different directions in the fracture model of Figure 8 (see details in Figure 9). For the front crack's propagation, for the sake of effective parallel channel effect, it is beneficiary for the front crack kinks into the free boundary direction as in Figures 3 and 4. Mathematically, this requires that $K_{II} < 0$ at the crack tip as in Figure 9a. Plug Eq. (5) into Eq. (4), we obtain the following relationship in Eq. (8).

$$\frac{tK_{II}\sqrt{h}}{F_X} = \frac{\sin(52.07^o)}{2\sqrt{2}} - \sqrt{6}\cos(52.07^o)\left(\frac{\beta_{YX} a}{h} - \frac{1}{4}\right) < 0$$
$$\to h < 2.30\beta_{YX} a \quad (8)$$

The result in Eq. (8) indicates that the parallel channel spacing h should be smaller than $2.3\beta_{YX} a$ for the front crack to be able to kink into the free channel. For typical sloping structure, we employ $\beta_{YX} = 0.5$ as a crude estimation (similar value has been employed previously (Bhat, 1988; Bhat et al., 1991; Lu et al., 2015a)). Based on this rather crude estimation, it is found that the spacing h and crack length a is in a ratio of 1:1.15 (or 0.8696:1).

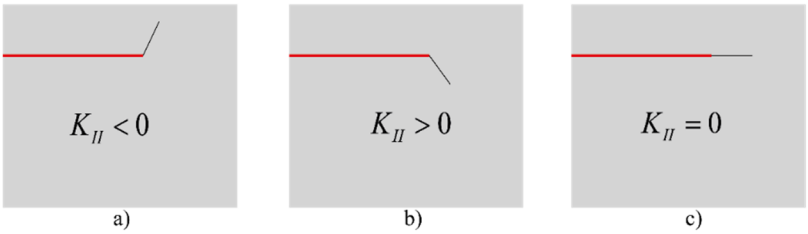

Figure 9. Kink direction and Mode-II SIF (after Thouless et al. (1987)).

On the other hand, for both scenarios in Figure 7, the Mode-II SIF $K_{II} > 0$ according to Eqs. (6), (7) and (4). This indicates that the side crack tends to kink into a direction away from the free boundary as in Figure 9b. This corresponds well with observations made in Figures 2 and 3, in which the side cracks kink into the ice floe instead of the free boundary.

Kink angle

With the knowledge of the sign of K_{II}, we made a rough but satisfactory estimation of the kink direction for both the front and side cracks. In this section, we further quantify the kink angle under different conditions. Eq. (4) quantified the Mode-I and II SIFs at the crack tip of $x = a$ in Figure 8. This physical crack tends to kink into a direction either with maximum energy dissipation or with a new purely Mode-I fracture mode (Anderson, 2005) (i.e., $k_{II} = 0$, see its definition in Eq. (9)). Usually both criteria yield negligible differences for all practical problems (Hutchinson and Suo, 1991). In this section, we first briefly present the theory adopted to analyse the crack kinking based on maximum energy release rate criterion. We assume that an infinitesimal crack kinks with an angle θ at the crack tip at $x = a$ in Figure 8. Based on stress field analysis, the new SIFs at the tip of the virtual infinitesimal crack, k_I and k_{II}, can be written as in Eq. (9).

$$\begin{aligned} k_I(\theta) &= C_{11}K_I + C_{12}K_{II} \\ k_{II}(\theta) &= C_{21}K_I + C_{22}K_{II} \end{aligned} \tag{9}$$

in which, the parameters are expressed in Eq. (10).

$$\begin{aligned} C_{11} &= 3/4\cos(\theta/2) + 1/4\cos(3\theta/2) \\ C_{12} &= -3/4[\sin(\theta/2) + \sin(3\theta/2)] \\ C_{21} &= 1/4[\sin(\theta/2) + \sin(3\theta/2)] \\ C_{22} &= 1/4\cos(\theta/2) + 3/4\cos(3\theta/2) \end{aligned} \tag{10}$$

The new energy release rate $G(\theta)$ at different kink angle θ can be written as in Eq. (11).

$$G(\theta) = \frac{k_I^2(\theta) + k_{II}^2(\theta)}{E} \tag{11}$$

in which,

$G(\theta)$ is the energy release rate at different kink angle [N/m];

E is the Young's modulus for sea ice [Pa].

Combining Eqs. (9), (10), and (11), we can identify the direction $\theta*$ towards which, maximum energy release rate is achieved.

4. RESULTS OF THEORETICLA MODEL STUDIES

Based on the observations made in Section 2, we introduced a fracture mechanic model to account for the in-plane fracture mechanisms of the parallel channel effect. This fracture mechanic model (in Figure 8) was further adapted to the side and front cracks' propagation models (in Figures 6 and 7 respectively). Based on this available fracture mechanic model, we further introduced the theory of crack kinking. Initial analysis in Section 3 shows that the chosen fracture model works in line with field observations. In this section, we further analyse the kink angle of different cracking events in Figures 8 and 9.

4.1 Kinking angle of front crack

In order to facilitate the analysis, we combine and further simplify Eqs. (4) and (5) in normalised forms as in Eqs. (12) and (13).

$$\begin{aligned}\frac{tK_I\sqrt{h}}{P} &= \frac{\cos(52.07^o)}{\sqrt{2}} + \sqrt{6}\sin(52.07^o)\left(\frac{2\beta_{YX}a}{h} - \frac{1}{2}\right)\\ \frac{tK_{II}\sqrt{h}}{P} &= \frac{\sin(52.07^o)}{\sqrt{2}} - \sqrt{6}\cos(52.07^o)\left(\frac{2\beta_{YX}a}{h} - \frac{1}{2}\right)\end{aligned} \tag{12}$$

$$\begin{aligned}\frac{tk_I\sqrt{h}}{P} &= C_{11}\left[\frac{\cos(52.07^o)}{\sqrt{2}} + \sqrt{6}\sin(52.07^o)\left(\frac{2\beta_{YX}a}{h} - \frac{1}{2}\right)\right]\\ &\quad + C_{12}\left[\frac{\sin(52.07^o)}{\sqrt{2}} - \sqrt{6}\cos(52.07^o)\left(\frac{2\beta_{YX}a}{h} - \frac{1}{2}\right)\right]\\ \frac{tk_{II}\sqrt{h}}{P} &= C_{21}\left[\frac{\cos(52.07^o)}{\sqrt{2}} + \sqrt{6}\sin(52.07^o)\left(\frac{2\beta_{YX}a}{h} - \frac{1}{2}\right)\right]\\ &\quad + C_{22}\left[\frac{\sin(52.07^o)}{\sqrt{2}} - \sqrt{6}\cos(52.07^o)\left(\frac{2\beta_{YX}a}{h} - \frac{1}{2}\right)\right]\end{aligned} \tag{13}$$

With varying kink angle θ, the calculations in Eq. (13) are presented in Figure 10 a and b with $\beta_{YX} = 0.5$. Different ratios between a and h were also investigated. Based on the results of Eq. (13), the energy release rate in different kink directions is quantified in Figure 10c according to Eq. (11). After retrieving the kink angle θ^*, we further studied the influence from the contact force ratios in Figure 10d. Figure 10 demonstrates that the kink angles of maximum k_I, zero k_{II} and maximum $G(\theta^*)$ appear to be in accordance with each other, as remarked by Hutchinson and Suo (1991). In the following sections, for simplicity, the maximum k_I criteria shall be adopted in studying the kink angle.

4.2 Kinking angle of side cracks

For numerical simplicity, we employed the same normalisation procedures to simplify Eqs. (6) and (7) into Eqs (14) and (15) respectively. The new normalised SIFs $tk_I\sqrt{h}/P$ and $tk_{II}\sqrt{h}/P$ at the kinked virtual crack tip can be obtained following the same procedures in Eq. (13).

For side crack scenario #1, $h > L_B + X_{side\_crack}$:

$$\begin{aligned}\frac{tK_I\sqrt{h}}{P} &= \frac{\cos(52.07^o)}{\sqrt{2}} - \sqrt{6}\sin(52.07^o)\left[\frac{1}{2} - \frac{(X_{side\_crack} + L_B)}{2h} + \frac{1}{2\beta_{YX}}\frac{a}{h}\right]\\ \frac{tK_{II}\sqrt{h}}{P} &= \frac{\sin(52.07^o)}{\sqrt{2}} + \sqrt{6}\cos(52.07^o)\left[\frac{1}{2} - \frac{(X_{side\_crack} + L_B)}{2h} + \frac{1}{2\beta_{YX}}\frac{a}{h}\right]\end{aligned} \tag{14}$$

For side crack scenario #2, $h \le L_B + X_{side\_crack}$:

$$\frac{tK_I\sqrt{h}}{P} = \frac{\cos(52.07^\circ)}{\sqrt{2}} - \sqrt{6}\sin(52.07^\circ)\frac{a}{2\beta_{YX}h}$$
$$\frac{tK_{II}\sqrt{h}}{P} = \frac{\sin(52.07^\circ)}{\sqrt{2}} + \sqrt{6}\cos(52.07^\circ)\frac{a}{2\beta_{YX}h} \quad (15)$$

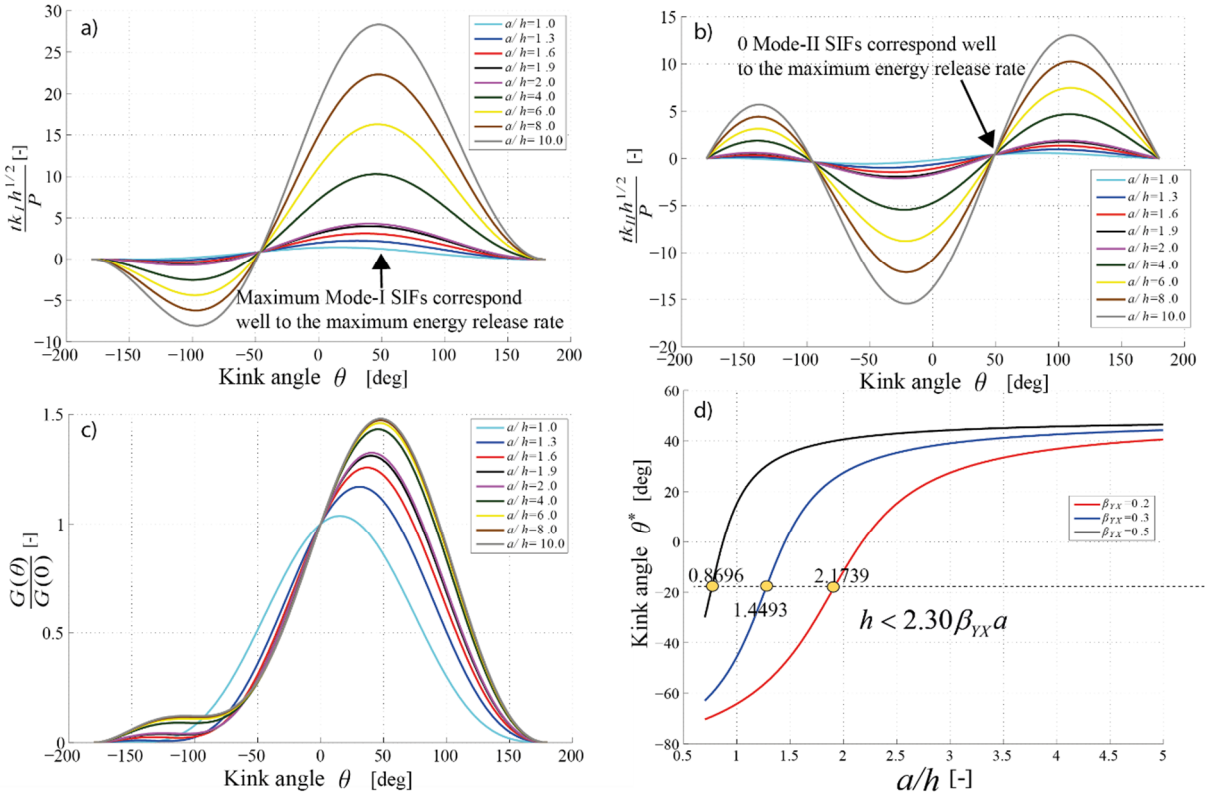

Figure 10. a) Normalised Mode-I SIF; b) Normalised Mode-II SIF; c) Normalised energy release rate at the virtual infinitesimal crack with varying kink angles; d) Kink angle versus ratio between crack length and channel spacing

Observing Eqs. (14) and (15), we see that the SIFs in both scenarios are influenced by the parameter β_{YZ} and the ratio between a and h. This is similar to the SIFs formulation of the front crack's propagation. Differently, Eq. (14) shows in addition a dependence on $(X_{side\_crack} + L_B)/h$, which signifies the influence from the location of side cracks' initiation in comparison to the bow size L_B and cracked floe width h (see Figure 7a).

We first presents the results of scenario #2 (see Figure 7b) described by Eq. (15). Following the concept of maximum k_I criteria, the normalised Mode-I SIF is plotted in Figure 11a with a special case of $\beta_{YX} = 0.5$. Afterwards, the influence of a/h and β_{YX} upon the side crack's kinking angle θ^* is presented in Figure 11b.

Then we present the result of Scenario #1 (see Figure 7a). The variation of normalised k_I is illustrated in Figure 12a with the special case of $\beta_{YX} = 0.5$ and $(X_{side\_crack} + L_B)/h = 0$. Then the kink angle θ^* is plotted versus a/h in Figure 12b. The influences from β_{YX} and $(X_{side\_crack} + L_B)/h$ were also accounted for.

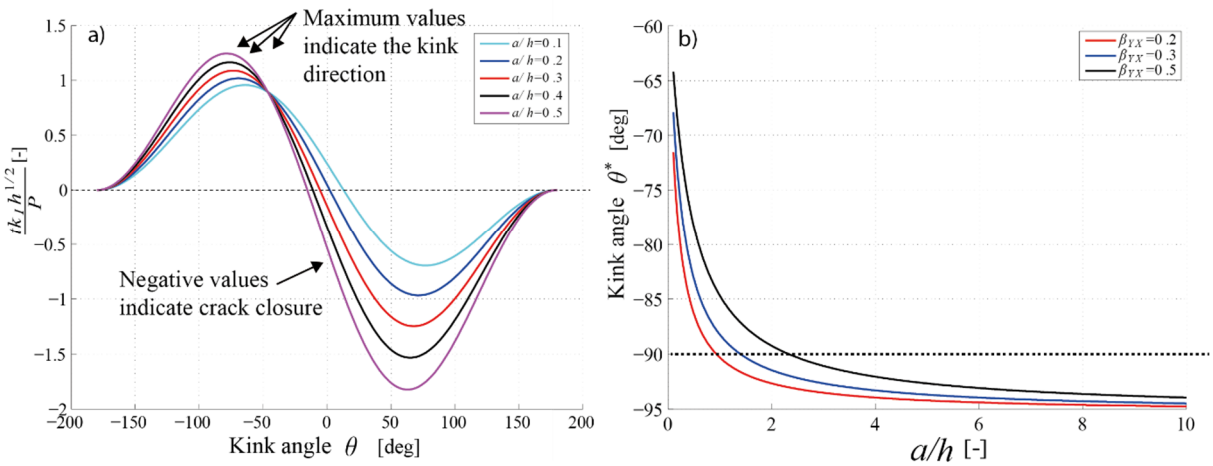

Figure 11. a) Normalised Mode-I SIF at the virtual infinitesimal crack with varying kink angles; b) Kink angle versus the ratio between 'crack length a (channel spacing)' and 'broken ice floe's dimension h in ship's length direction for theoretical model in Figure 7b.

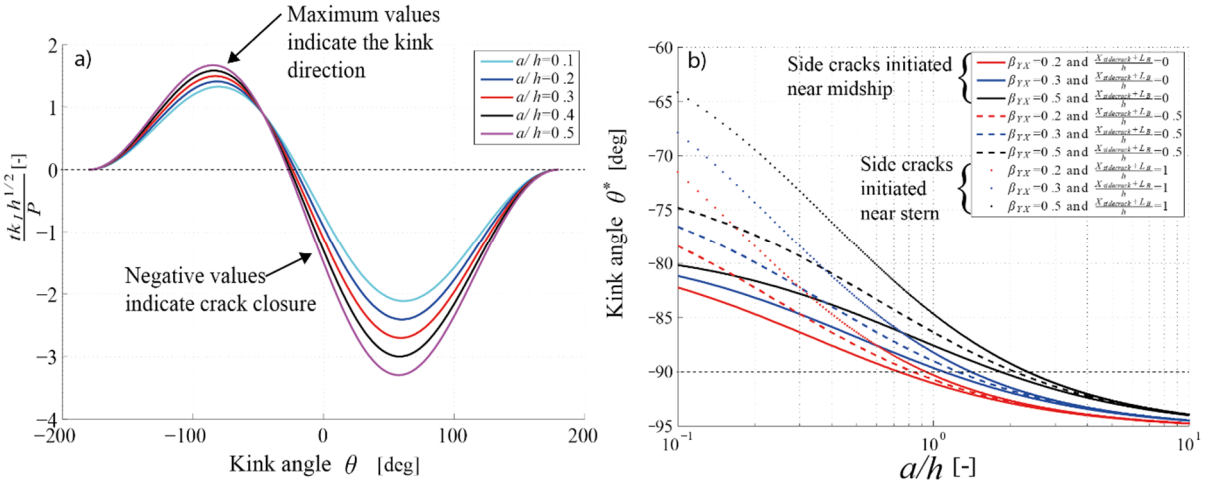

Figure 12. a) Normalised Mode-I SIF at the virtual infinitesimal crack with varying kink angles; b) Kink angle versus the ratio between 'crack length a (channel spacing)' and 'broken ice floe's dimension h in ship's length direction' for theoretical model in Figure 7a.

5. DISCUSSIONS

5.1 Front crack's propagation and aspect ratios of broken ice floes

For the front crack's propagation model in Figure 6, calculation results in Figure 10 shows that the front crack's kink angle θ^* is around 50° towards the nearby free channel. This kink angle is in line with the observations made in Figures 3 and 4.

The optimum kink angle is influenced by the ratio of a/h. Particularly for the front crack scenario in Figure 6, a/h stands for the ratio between 'the length of the front crack before kinking' and 'the spacing between parallel channels'. It is also indicative to the aspect ratio of broken ice pieces in between the parallel channels. The detailed influence of a/h upon θ^* is illustrated in Figure 10d. We see that a certain threshold value has to be exceeded in order for the front crack to kink into the nearby free channel (i.e., $\theta^* > 0$). A criteria deduced in Eq. (8) is further confirmed in Figure 10d, i.e., a/h should be larger than $1/(2.30\beta_{YX})$ in order to enhance the parallel channel effect from the originally straight front crack. As we have mentioned above, a/h also stands for the aspect ratio of broken ice floes in between the parallel

channel. Using $\beta_{YX} = 0.5$ as a crude estimation, it turned out that broken floe sizes with aspect ratio $a/h > 0.8696$ are expected. This value is in line with Hamilton et al.'s (2011a) assumption that broken ice floes of a 1:1 aspect ratio were generated in between the parallel channels.

5.2 Side cracks' propagation and aspect ratio of broken ice floes

Two different scenarios were studied separately for the side cracks' propagation. However, the results of these two scenarios were rather similar according to the calculations presented in Figures 11 and 12. In both scenarios, the crack tends to kink away from the free boundary (i.e., $\theta^* < 0$). This is mainly due to the presence of negative turning moment leading to a positive K_{II} value at the physical crack tip. The kink angle θ^* rapidly converges to a value around -90° as the ratio a/h increases. This kinking angle is again in good agreement with the field observations documented in Figure 2, in which the side crack's kink angle is almost 90° irrespective of influences from irregular boundaries.

The ratio of a/h in the side cracks' propagation model (see Figure 7) has a different meaning comparing with the case of front crack as discussed above. For the side crack propagation model, the parallel channel spacing is reflected by the value of a whereas h represents a dimension which is in the ship length direction (see Figure 7). Both Figures 11 and 12 shows that at smaller a/h values, the side crack kinks with a relatively smaller angle θ^* (-65°~-80°). Once the ratio a/h becomes larger than 1 or 2 (depending on the value of β_{YX} and $(X_{side\_crack} + L_B)/h = 0$), the kink angle θ^* reached 90° already. This, in a way, indicates that the parallel channel spacing a for side cracks' propagation problem should be smaller $2h$ to alleviate the unfavourable kinking direction inherent with side cracks (i.e., having $a/h \le 2$ in order for $\theta^* > -90^\circ$). This indicates that the aspect ratios of broken ice floes generated in between two parallel channels by the side crack are expected to be larger than 1:2 (i.e., $h/a \ge 1:2$). If we look into Figure 2, following one of the side cracks, the distance from ODEN to the kink point (i.e., a) is almost twice of the width of this broken ice piece (i.e., h). Similar relationship can also be found in Figures 3 and 4, in which, side cracks were also present.

5.3 Size of broken ice pieces generated in between parallel channels

We examined the possible broken ice floes' aspect ratio left in between two parallel channels with the fracture mechanic model in Figure 8. Rather satisfactory agreements were achieved between the theoretical model and field observations even though the irregular boundaries and inhomogeneity of sea ice were not accounted for by the theoretical model. However, the practical questions regarding the 'optimum parallel channel spacing' and accordingly the out-going floe size have not yet been answered thus far. In order to answer these questions, we need to further solidify one of the numbers between a and h. Since their probable ratio has been established in this paper, any one of these two numbers is known, the optimised parallel channel spacing and out-going broken floe size are therefore acquired. In order to obtain this information, we need to collectively evaluate the side and front cracks' driving force P (see definitions in Eqs. (6) and (7)) and the local out-of-plane failure force (Lu et al., 2015e; Lu et al., 2015h). This shall be studied in a separate paper. Thus far, we have only constructed the information regarding the ratio of a/h depending on different failure mechanisms.

5.4 Limitations

Apart from not being able to quantify the exact optimum parallel channel spacing, the theoretical model proposed in this paper has also neglected several important features such as irregular floe geometry and inhomogeneity of sea ice. Most importantly, this theoretical model (in Figure 8) was derived from beam theory following energy principles (Thouless et al., 1987).

Thus the applicability of beam theory can be questioned. In spite of all these shortcomings, this theoretical model (Figure 8) demonstrates surprisingly good resemblance to field observations in Section 2. Further numerical analysis is needed to investigate the accuracy and applicability of this theoretical model in the current application.

6. CONCLUSION

In view of the parallel channel effect in reducing floe sizes in between two parallel channels, we seeks to offer tentative theoretical explanations to its fracture mechanisms. This is a first step towards addressing practical problems such as 'optimised parallel channel spacing' and 'out-going floe sizes' after certain ice management operations.

Field tests in relation to parallel channel tests have been conducted with extensive panoramic images. Based on the field observations, we draw the following qualitative conclusions:

- With the presence of a free boundary nearby a transiting icebreaker, long cracks start to emanate around the bow area. Very few cracks were initiated from mid-ship or astern;
- Ice fractures in a variety of patterns, among which, two types of fracturing pattern (side and front cracks) have been repetitively observed;
- The side cracks show a tendency to kink into the large ice floe. For narrow spacing, the side crack can just propagate through and reach the free boundary;
- The presented front crack shows a strong tendency to kink into the free boundary direction.

Based on the observations, we believe that both the side cracks and the kinking behaviour of front cracks are among the most important failure mechanisms behind the parallel channel effect. Two idealised theoretical models have been proposed to study the propagation of side and front cracks respectively. These two theoretical models were essentially rooted in a same fracture mechanic model. This theoretical model offers analytical solutions of the mixed model Stress Intensity Factors at the physical crack tip. Following both the maximum energy release rate and maximum Mode-I fracture criteria, we analysed the kink angle of both the front and side cracks. The results obtained through theoretical analysis are in good agreement with field observations. Based on the theoretical analysis, the following quantitative conclusions can be drawn:

- In order for front crack to kink into the free channel, it is generally required that Mode-II Stress Intensity Factor at the crack tip $K_{II} < 0$;
- The above criteria leads a requirement that the ratio between 'the front crack's length' and 'the parallel channel spacing' should be larger than $1/(2.30\beta_{YX})$. β_{YX} is defined in Eq. (2) representing the contact force ratio in Y and X direction (see Figure 5);
- The above-mentioned ratio is indicative of the aspect ratio of broken ice floes left in between two parallel channels if front cracks successfully intersect the solid ice in between. This means that broken ice floes of an aspect ratio larger than $1/(2.30\beta_{YX})$ are expected. As a crude approximation, utilising $\beta_{YX} = 0.5$ leads broken ice floes' aspect ratios are in the range of larger than 1:1.15 (or 0.8689:1), which is in accordance with Hamilton et al.'s (2011a) assumption of 1:1 aspect ratio;
- With $K_{II} < 0$ and a large above-mentioned ratio, the front crack tends to kink towards the free channel with an angle around 50°, which agrees well with field observations;
- Side cracks showed a consistent tendency to kink away from the free channel due to the positive Mode-II Stress Intensity Factor at the crack tip $K_{II} > 0$;
- Side cracks' kink angle shows a strong tendency to converge to around -90°. Such a sudden 90° kinking behaviour has been frequently observed in the field;

- Milder kink angle (e.g., -65^{o}) is encouraged to enhance the parallel channel effect of side cracks. Achieving such condition indicates that the broken ice floes' aspect ratios are in a range of larger than 1:2.

All these quantitative numbers can be substantiated by the field observations. This is encouraging for the currently chosen theoretical model. Further inclusions of force calculation shall be conducted to evaluate the optimum parallel channel spacing. In addition, numerical validation of the current theoretical model is also necessary.

ACKNOWLEDGEMENT

The authors would like to thank the Norwegian Research Council through the research centre SAMCoT CRI for financial support and all the SAMCoT partners. In addition, funding from Statoil for the OATRC 2012 and 2013 research cruise is highly appreciated. Dr. Anatoly Sinitsyn and Dr. Francesco Scibilia's initiatives in using and Bjørklund Henrik's excellent job in mounting and processing 360 degree camera system are also highly regarded.

REFERENCES

Anderson, T.L., 2005. Fracture mechanics: fundamentals and applications. CRC press.

Bhat, S.U., 1988. Analysis for splitting of ice floes during summer impact. Cold Regions Science and Technology, 15(1): 53-63.

Bhat, S.U., Choi, S.K., Wierzbicki, T. and Karr, D.G., 1991. Failure analysis of impacting ice floes. Journal of Offshore Mechanics and Arctic Engineering, 113: 171.

Bjørklund, H., Sinitsyn, A. and Prusakov, A., 2015. 360 Camera System for Mornitoring Ice Conditions, Proceedings of the 23rd International Conference on Port and Ocean Engineering under Arctic Conditions, Trondheim, Norway.

Farid, F., Scibilia, F., Lubbad, R. and Løset, S., 2014. Sea Ice Management Trials during Oden Arctic Technology Research Cruise 2013 Offshore North East Greenland, 22nd IAHR International Symposium on Ice, Singapore.

Gold, L.W., 1971. Use of ice covers for transportation. Canadian Geotechnical Journal, 8(2): 170-181.

Hamilton, J., Holub, C., Blunt, J., Mitchell, D. and Kokkinis, T., 2011a. Ice Management for Support of Arctic Floating Operations, OTC Arctic Technology Conference.

Hamilton, J., Holub, C.J. and Blunt, J., 2011f. Simulation of ice management fleet operations using two decades of Beaufort Sea ice drift and thickness time histories, Proceedings of International Society of Offshore and Polar Engineers (ISOPE), Maui, Hawaii.

Hutchinson, J.W. and Suo, Z., 1991. Mixed mode cracking in layered materials. Advances in applied mechanics, 29: 63-191.

Kerr, A.D., 1976. The bearing capacity of floating ice plates subjected to static or quasi-static loads. Journal of Glaciology, 17: 229-268.

Lu, W., 2014. Floe Ice - Sloping Structure Interactions. Doctoral Thesis, Norwegian University of Science and Technology, Trondheim.

Lu, W., Lubbad, R. and Løset, S., 2015a. In-plane fracture of an ice floe: A theoretical study on the splitting failure mode. Cold Regions Science and Technology, 110(0): 77-101.

Lu, W., Lubbad, R. and Løset, S., 2015e. Out-of-plane failure of an ice floe: radial-crack-initiation-controlled fracture. Cold Regions Science and Technology.

Lu, W., Lubbad, R., Løset, S. and Kashafutdinov, M., 2015h. Fracture of an ice floe: Local out-of-plane flexural failures versus global in-plane splitting failure. Cold Regions Science and Technology.

Lubbad, R., 2012. Data report: KV-Svalbard Survey 2012, Faculty of Engineering Science and Technology (IVT), NTNU, Trondheim.

Lubbad, R. and Løset, S., 2011. A numerical model for real-time simulation of ship-ice interaction. Cold Regions Science and Technology, 65(2): 111-127.
Lubbad, R., Løset, S. and Lu, W., 2012. Oden Arctic Technology Research Cruise 2012: Data report Part I, SAMCoT report, Norwegian University of Science and Technology, Trondheim.
Lubbad, R., Løset, S. and Lu, W., 2013a. Oden Arctic Technology Research Cruise 2013: Field-Data report, Norwegian University of Science and Technology, Trondheim.
Lubbad, R., Raaij, E.V., Løset, S. and Eik, K.J., 2013b. Oden Arctic Technology Rsearch Cruise 2012, Proceedings of the 22nd International Conference on Port and Ocean Engineering under Arctic Conditions, Espoo, Finland.
Nevel, D.E., 1958. The theory of a narrow infinite wedge on an elastic foundation, U. S. Army Snow Ice and Permafrost Research Establishment, Corps of Engineering.
Nevel, D.E., 1961. The narrow free infinite wedge on an elastic foundation, U. S. Army Snow Ice and Permafrost Research Establishment, Corps of Engineering.
Nevel, D.E., 1965. A semi-infinite plate on an elastic foundation, U. S. Army Snow Ice and Permafrost Research Establishment, Corps of Engineering.
Scibilia, F., Metrikin, I., Gürtner, A. and Teigen, S.H., 2014. Full-scale trials and numerical modeling of sea ice management in the greenland sea, OTC Arctic Technology Conference. Offshore Technology Conference.
Sodhi, D.S., 1996. Deflection Analysis of Radially Cracked Floating Ice Sheets, OMAE, pp. 97-102.
Thouless, M.D., Evans, A.G., Ashby, M.F. and Hutchinson, J.W., 1987. The edge cracking and spalling of brittle plates. Acta Metallurgica, 35(6): 1333-1341.